# Flat-Ended Circular Cylinder in Hypersonic Rarefied Flow

J. K. Harvey,* M. C. Celenligil,† R. G. Dominy,‡ and M. R. Gilmore§
*Imperial College, London SW7, England, United Kingdom*

**The paper describes a study of the rarefied hypersonic flow about a flat-ended circular cylinder at various angles of attack. Examples of direct simulation Monte Carlo (DSMC) calculations for nonreacting nitrogen flows are presented, covering a range of Knudsen numbers from 0.034 to 1.84. These include the effects of rotational and vibrational energy exchange. Contour plots of density and temperature show the structure of the disturbed flowfield. For zero angle-of-attack flows, the density and rotational temperature predictions are compared with measurements made in a hypersonic wind tunnel at a Mach number of about 25 for a range of Knudsen numbers. Close agreement between the two is seen, although a lag in rotational temperature suggests that the coupling to this mode is underestimated. The DSMC calculations have been extended to cover angles of attack up to 40 deg. Flowfield and surface flux patterns are presented for these cases. For the denser flows, the maxima in heat transfer occur away from the plane of symmetry.**

## Nomenclature

$E_{cm}$ = center of mass energy
$Kn$ = Knudsen number, $\lambda_\infty/R$
$M$ = Mach number
$R$ = cylinder radius
$St$ = Stanton number
$T$ = temperature
$x,r$ = coordinates
$\lambda$ = mean free path
$\rho$ = density
$\phi$ = exchange restriction factor

*Subscripts*
$\infty$ = freestream conditions
rot = rotational
tr = translational
vib = vibrational
wall = wall conditions

## Introduction

THIS paper presents a study of the rarefied hypersonic flow about a flat-ended circular cylinder at various angles of attack. The flow conditions are typical of those experienced by spacecraft at altitudes above 65 km, that is, those associated with the transitional flow regime, which is characterized by the Knudsen number $Kn$ being the order of 0.01 or larger. In these circumstances, the degree of molecular nonequilibrium is such that the Navier-Stokes equations are inappropriate. Reliable numerical prediction can, however, be made by the now well-established direct simulation Monte Carlo (DSMC) method, devised by Bird,[1] which seeks solutions for the flowfields at a molecular level. This has been demonstrated to be an accurate and versatile technique for rarefield nonequilibrium flows,[2] and the evidence from the comparisons between experiments and calculations presented in this paper adds further credence to this notion.

Although the flat-ended cylinder is not a shape that has general direct applicability to spacecraft, it was chosen for this study to test the DSMC method in a situation of rapid compression. An enlarged area of near-stagnation flow is developed in the region ahead of the front of the cylinder, making it easier to resolve the details of the compression process and the relaxation toward an equilibrium state in both the computations and experiments. Some of the data presented in this paper have already been included in work by Harvey.[3] Here further experimental results and more comprehensive calculations are given, including data for the cylinder at angles of attack.

This study is concerned with flows that are chemically nonreacting. The experiments and calculations were performed for pure nitrogen at temperatures where the only significant real gas effects were those associated with internal and translational energy exchange. The calculations have been performed for a gas in which both rotational and vibrational energy exchange has been included. Generally, in nonreacting upper atmosphere flows, the vibrational mode is considered to be effectively frozen because the coupling between this and the rotational and translational modes is very weak. In the present example, because the stagnation region is enlarged, the molecules dwell there long enough for vibrational exchange to have some influence on the flow evolution. In chemically reacting flows, the level of vibrational excitation, or, to be more precise, the population of individual quantum levels of this mode, determines the probability of a reaction taking place. The vibrational mode also plays an important role in absorbing energy after a reaction collision. This has been the motivation for the testing of vibration routines in connection with the DSMC codes.

## Direct Simulation Monte Carlo Method

### General

In the DSMC method, it is assumed that the motion of several thousand sample particles can adequately represent, in a statistical way, the behavior of the far larger number of particles within a real flowfield. The simulation is performed in real time within a framework of cells in physical space and the sample particles carry with them the phase-space information of species, position, velocity, and internal energy that is necessary for the true evolution of a flowfield to be constructed. The method produces solutions analogous to those of the Boltzmann equation. These solutions are obtained by decoupling the Boltzmann collision and convection terms by

Presented as Paper 89-1709 at the AIAA 24th Thermophysics Conference, Buffalo, NY, June 10–14, 1989; received Oct. 3, 1989; revision received Feb. 16, 1990; accepted for publication Feb. 26, 1990.


*Professor of Gas Dynamics, Department of Aeronautics. Member AIAA.
†Research Assistant, Department of Aeronautics; currently, Lecturer, University of Ankara, Ankara, Turkey.
‡Research Assistant, Department of Aeronautics; currently Department of Engineering and Applied Science, University of Durham, Durham, England, UK.
§Research Assistant, Department of Aeronautics.

means of a suitable small step time-discretization. Each term is calculated alternately and independent of the other at the successive time intervals. These are chosen to be small compared with the time taken for representative particles to traverse any cell. The method is now well known; the reader is referred to cited texts, in particular, Bird,[1] for further discussion.

Many solutions exist within the literature using the DSMC method for rarefied flows, mostly for high incident Mach numbers. The method has the advantage of being almost unrestricted in the complexity of a flow that can be analyzed given sufficient computing power. Flows with internal energy exchange, chemical reactions, and ionization can be predicted if suitable models for the intermolecular collisions can be provided. Since the routines for handling the collisions will be called many millions of times in a typical flowfield calcualtion, they must be very efficient, and, in practice, a compromise between rigor and simplicity has to be made.

#### Collision Model

The present paper is concerned with flows of a single species gas, molecular nitrogen. The range of temperature used in both the computations and the experiments has been restricted below the level where dissociation occurs.

Davis et al.[4] and Macrossan[5] review a number of options that are open for the DSMC modeling of collisions that involve the internal energy exchange. These interaction models have two functions to perform: 1) to determine the postcollision scattering and 2) to establish the redistribution of energy between the translational and internal modes. Apart from the first interactions between the freestream particles and ones already influenced by the body, the orientation of each collision within the disturbed part of a typical hypersonic flowfield is essentially random. Thus, the sensitivity to the choice of the scattering model can be expected to be minimal. This has been borne out by comparative tests by Macrossan.[5] For the calculations presented in this paper, monatomic spherical scattering, independent of the internal energy, will be used. The scattering is calculated using either a Morse potential or a variable hard sphere (VHS) inverse power model.[6] The intermolecular force for the latter is wholly repulsive, whereas the former also includes a more realistic long-range attractive force that influences the low relative velocity and high miss-distance scattering in particular. The physical constants used in the models have been chosen to give the best match between the Chapman-Enskog viscosity and measured values (see Davis et al.[4]).

The model that has been used throughout the work to calculate the interchange between the internal and translational energies has been developed from the original concepts of Borgnakke and Larsen[7] and Larsen and Borgnakke[8] (the latter designated B&L-2). By random selection from appropriate distributions, these models use a statistical $\beta$ function formulation to predict the way in which the energy is shared between each mode after a collision. Davis[9] and Pullin[10] have proposed alternatives to the B&L-2 scheme in which the interchange of rotational energy for each collision is dependent on the center of mass energy; the degree of coupling thus varies with gas temperature rather than exhibiting the less realistic fixed rotational relaxation number of the B&L-2 scheme. These models also satisfy detail balance, whereas B&L-2 does not.

The present calculations have been made using a model in which rotational and vibrational exchanges are simulated. For the former, Davies' rotational scheme is used for which the exchange restriction factor (the fraction $\phi$ of energy elastically scattered during each encounter) is given by the expression

$$\phi_{\text{rot}} = 0.148 + 1.018 \exp(-0.001722 E_{cm} T_\infty)$$

where $T_\infty$ is a nominal temperature set equal to 11.75 K and $E_{cm}$ is the center-of-mass energy relative to the gas at $T_\infty$. Relaxation simulations give close agreement with Carnevale et al.'s[11] measured form of the variation of the relaxation times with temperature. The coefficients have been chosen to give the best fit to this data. A corresponding expression for the vibrational exchange restiriction factor has been derived using an analogous method to Davies. The equivalent vibrational exchange restriction factor is given by

$$\phi_{\text{vib}} = 7.5/(0.49 T_\infty E_{cm} + 1377)$$

The factor $\phi_{\text{vib}}$ is a small number reflecting the small fraction of vibrational energy available for exchange in each encounter, which is consistent with the observed weak vibrational-translational coupling of nitrogen. The model presupposes that the scattering into and out of the two internal modes is uncorrelated and individually dependent on the center-of-mass energy. The coefficients for the vibrational case have been empirically derived from comparisons between relaxation simulations covering a range of temperatures and the data from Refs. 12–14.

## Computations

#### Axisymmetric Flows

Calculations of the flow about the circular flat-ended cylindrical body at zero angle of attack have been made using an axisymmetric DSMC code for Mach numbers of around 25. The calculations cover a range of Knudsen numbers $Kn$ ranging from 0.03 to 1.84. Further calculations, in which the body has been set at angles of attack up to 40 deg, have also been completed for Knudsen numbers of 0.065 and 1.84. In all cases, rotational excitation has been included, but vibrational excitation has been activated for selected runs only. The usual computational precautions, including ensuring that there are sufficient particles and cells have been adhered to throughout the calculations. The values of the freestream conditions and the model temperatures used in the calculation are given in Table 1.

The typical way in which the rarefied flows differ from the continuum pattern can readily be seen from Fig. 1, in which contours of density (normalized with respect to the freestream value) are shown for the body at zero angle of attack for a Knudsen number of 0.0645. Over the whole of the front face, an increasingly rapid rise in density is observed as the flow approaches the body. Although the flow is moderately dense, in-

**Table 1 Flow conditions for data presented in the figures**

| Figure | $Kn$ | $M_\infty$ | $T_\infty$ | $T_{\text{wall}}$ | Expt/comp |
|---|---|---|---|---|---|
| 1 | 0.0645 | 24.74 | 11.69 | 375.0 | C |
| 2 | 0.0645 | 24.7 | 11.69 | 375.0 | C |
| | 1.84 | | | | |
| 3 | 0.061 | 24.7 | 11.69 | 375.0 | C |
| | 1.840 | | | | |
| 5 | 0.106 – | 25.0 | 16.45 | 351.0 | E |
| | 0.065 | | | | |
| 6 | 0.095 – | 25.6 | 16.51 | 352.0 | E |
| | 0.045 | | | | |
| 7 | 0.072 | 24.4 | 20.12 | 351.0 | E&C |
| 8 | 0.085 | 25.4 | 16.51 | 352.0 | E&C |
| 9 | 0.046 | 25.9 | 15.49 | 345.8 | E&C |
| 10 | 1.40 | 25.4 | 16.2 | 345.8 | E |
| | 0.34 | 25.5 | 16.2 | 347.2 | E |
| | 0.15 | 25.1 | 16.2 | 347.2 | E |
| | 1.84 | 24.7 | 11.69 | 375.0 | C |
| | 0.106 | 25.0 | 16.45 | 351.0 | C |
| | 0.085 | 25.33 | 16.5 | 362.2 | C |
| 11 – 16 | 0.0645 | 24.74 | 11.64 | 375.0 | C |
| 17 | 1.84 | 24.74 | 11.64 | 375.0 | C |
| 19 | 0.034 | 21.3 | 17.1 | 377.0 | C&E |
| 20 | 0.043 | 21.3 | 17.1 | 377.0 | C&E |

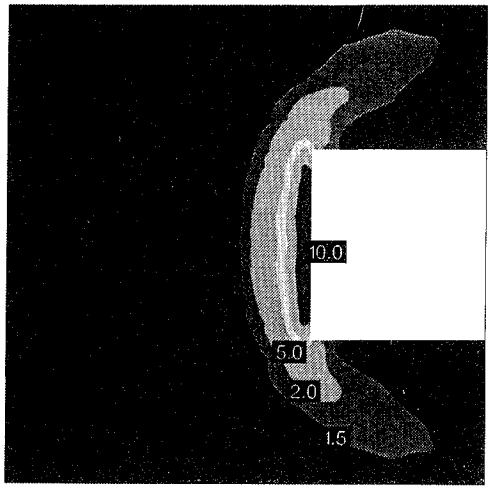


**Fig. 1 Normalized density contours ahead of a blunt cylinder at zero angle of attack; $M = 24.74$, $Kn = 0.0645$.**

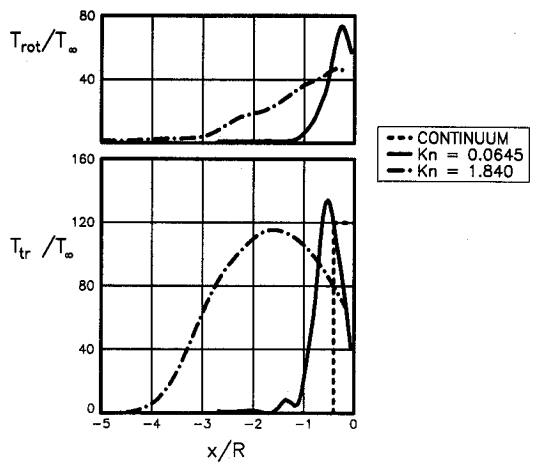


**Fig. 2 Temperature profiles along the stagnation streamline; $M = 24.74$.**

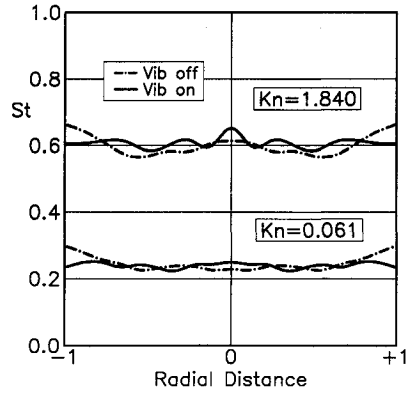


**Fig. 3 Effect of including vibrational exchange on the heat transfer to the front face of the cylinder at Mach 24.74.**

stead of there being a discrete shock wave, complete merging of the shock with the nonequilibrium viscous flow adjacent to the solid surface is seen. The magnitude of the peak in density is considerably higher than the equivalent Rankine-Hugoniot value, which would have been about six times the freestream value. The shock layer thins slightly as it spreads out away from the axis until it reaches the corner of the body, where it expands rapidly as it flows back along the side of the cylinder. However, it is some distance along the body before the density falls below the freestream value. An attenuated and non-Rankine oblique bow shock propagates outward into the surrounding flow from a point a little ahead of the corner.

Figure 2 shows translational and rotational temperature profiles of the approaching flow along the axis for two Knudsen numbers. It is evident by comparison with Figs. 1 and 5 that for the $Kn = 0.0645$ example, the translational temperature component rises to a peak well before any substantial increase in density has been experienced. The same is true for the more rarefied example shown in Fig. 2. This rise is due to particles being reflected forward from the compression region into the low-density approaching flow. Energetic collisions between the fast moving freestream particle and reflected ones result in the translational temperature rising to a peak comparable in magnitude to that behind the bow shock for the equivalent continuum flow. Because of the scarcity of collisions in the region of low density up to the temperature peak, there is only weak coupling between the translational and internal modes. The rotational temperature thus remains well below the translational value and only slowly climbs until the proximity of the cold front face of the body causes both to drop. As the flow approaches the stagnation point, the combination of the sharp rise in density and the fall in flow velocity allows sufficient collisions to occur for equilibrium to be approached, and even the vibrational temperature, which up till now is essentially frozen, rises toward the wall temperature.

Calculations have been made with vibrational exchange inhibited, and it is interesting to observe the effect on the heat transfer to the front face of the body. In Fig. 3, distributions of Stanton number for two Knudsen numbers (1.84 and 0.061) are shown with and without vibrational exchange. For both Knudsen numbers, the distributions are roughly flat but rise slightly toward the perimeter when vibration is frozen. With vibrational exchange activated, one would expect the particles in the vicinity of the stagnation point to remain long enough for there to be a transfer of energy to and from this mode. Energy absorbed into vibration in the shock layer would be recovered adjacent to the wall and, consequently, the heat transfer would be increased over the center portion of the front face in comparison with the vibrationally frozen value. In the examples cited, the denser case shows no increase at the stagnation point. The more rarefied flow appears to show an increase at the stagnation point, but this is probably within the expected statistical scatter and is not thought to be proof that there is an effect from unfreezing the vibrational mode.

### Angle-of-Attack Flows

Computations made using a three-dimensional DSMC code are presented for the flow about the blunt cylinder at angles of attack up to 40 deg. This code is similar to the axisymmetric version used for the zero angle-of-attack examples, except for the type of cell geometry that is used. The cells are cuboids, subdivided into tetrahedrons, whereas those used for the axisymmetric calculations are quadrilateral. The same intermolecular collision models are available and a Morse potential scattering routine has been used in the examples cited, which are for two Knudsen numbers (0.065 and 1.84).

## Experiments

### Wind Tunnel

The experimental measurements were made in the Imperial College graphite-heated, nitrogen wind tunnel. This is a continuously running blowdown tunnel with a circular 200-mm-diam working section where freestream Mach numbers in the range of 18 to 25 are typical. The working gas is pure nitrogen. To ensure constant and steady reservoir conditions, servo-systems control the flow of gas and the power supplied to the heater. The wind tunnel has a contoured liquid-nitrogen-cooled nozzle. This produces a flow with negligible Mach

number gradients as far as the 10-mm diam model is concerned. Stagnation temperatures of up to 3000 K can be generated at pressures betweeen 3 and 70 MPa. However, the tests were performed for reservoir temperatures of between 1270 and 1650 K. Full details of the facility are given by Dominy.[15]

**Electron Beam Fluorescence Measurements**

All of the flowfield measurements cited were obtained using the electron beam fluorescence technique (EBFT). A well-collimated beam of electrons was fired through the flow from a 30-kV source located outside the test section. In the rarefied nitrogen environment, this gave rise to a fluorescent beam a little under 1 mm in diameter that could be used for density and rotational temperature studies.

The most convenient way of introducing the beam into the flow is to fire it from the side of the test section across the face of the model. Secondary electrons that have a larger collision cross section than the primaries make an important contribution to the fluorescence. The close proximity of the grounded model surface is likely to influence the distribution of these slower-moving particles sufficiently to invalidate the intensity-density calibrations. For this reason, a different beam path was chosen (see Fig. 4). The electrons were deflected magnetically behind the model so as to pass through it and emerge from a small hole in the front face in a direction parallel to the undisturbed flow. Introducing the beam this way caused a minimal distortion of the secondary electron cloud.

The blunt-ended cylindrical models used for the tests were constructed from tellurium-copper and were water cooled, maintaining the surface temperature at, typically, 375 K. The diameter of the model used for the majority of the experiments was 10 mm, and was designed with a smaller center cylindrical core through which the electron beam was guided. The outer part of the model was an eccentric collar that could be rotated, thus moving the axis of the body while keeping the electron beam position unchanged. This allowed off-axis surveys to be carried out. Inside the model, immediately behind the face, was a cavity that was supplied with nitrogen to balance the surface pressure and prevent flow through the electron beam guide hole.

Density profiles were obtained by measuring the total intensity of the O-O band of the first negative system of the nitrogen spectrum. The optical arrangement (see Fig. 4) for observing the fluorescence achieved a resolution of 0.15 mm in the direction perpendicular to the model surface. When performing a traverse along the beam, it was momentarily turned off between each reading by magnetic deflection, to ensure frequent and accurate photometric assessments of the dark current and correction for stray light. All data were normalized with respect to the freestream density measured upstream of the body flowfield. The readings were also normalized with respect to the current in the emerging beam.

Rotational temperature spectra were recorded using a Spex 1-m spectrometer and a similar quartz lens and fiber optical system to that used for the density. Because of the very low light intensity of the fluorescence and the high dispersion of the spectrometer, digital filtering techniques were necessary to improve the signal-to-noise ratio. The spectrometer was fitted with a moveable outlet slit that could be traversed through the required wavelength range. By repeatedly scanning the spectrum at about 1 Hz for 15 min and superimposing digitally the resultant signal traces, very good resolution of the R-branch of the $N_2^+$ (O-O) band was achieved. Superposition of many samples of the spectrum averages the noise component to a diminishing small value since it is random. In contrast, the required spectrum sums towards its true value. Further enhancement of the spectrum was achieved by matching it numerically to a "best fit" theoretical profile in which the optical "profile" of the instrumentation was accounted for. An iterative technique was used to predict and subtract the contribution from the overlapping P-branch. Inferred values of the rotational temperature were calculated using the scheme devised by Smith.[13] At the level of temperature used in these tests, which was generally below 1000 K, the effect of the relative increase in the population of the higher vibrational levels due to rising temperature, and hence reduction of the (O-O) branch intensity, is insignificant (see Cattolica et al.[17]).

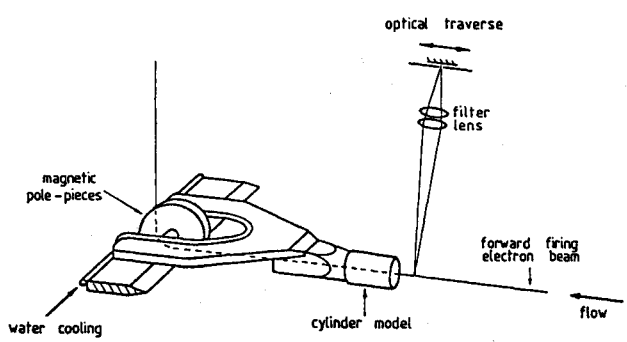


**Fig. 4 Arrangement used to make the electron beam fluorescence measurements ahead of the model's front face.**

## Results

**Density**

Density profiles measured ahead of the front face of the body for a range of Knudsen numbers are shown in Figs. 5 and 6. Examples are given along the axis of symmetry and near the edge of the body ($r/R = 0.85$). Although there is a 2:1 change

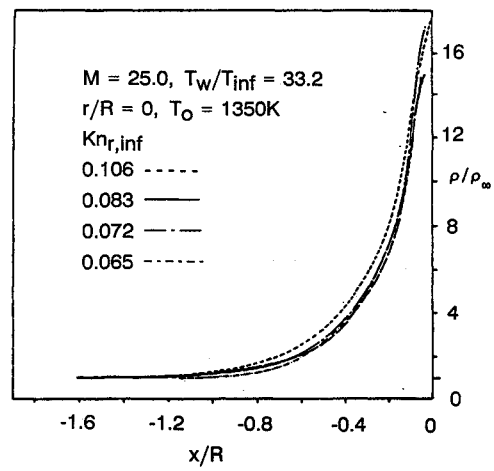


**Fig. 5 Measured density profiles ahead of the body at different Knudsen numbers at zero angle of attack along the axis.**

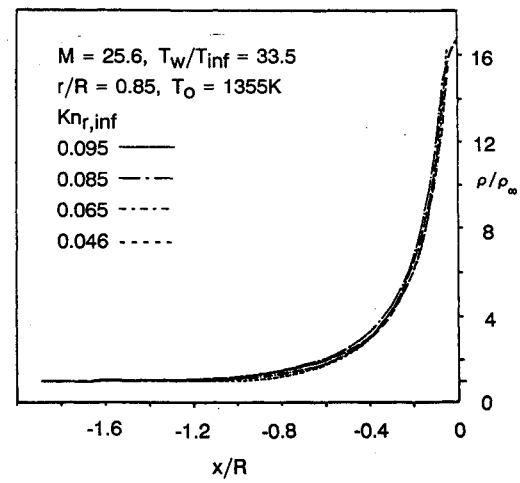


**Fig. 6 Measured density profiles obtained "off axis."**

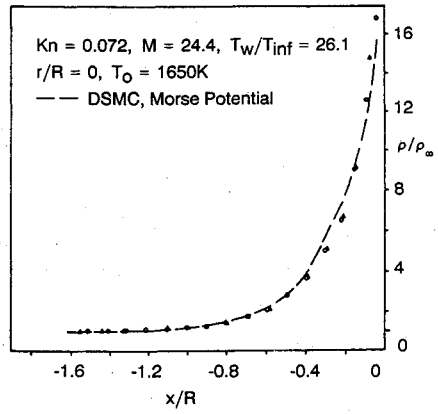


**Fig. 7 Measured and predicted density profiles along the axis.**

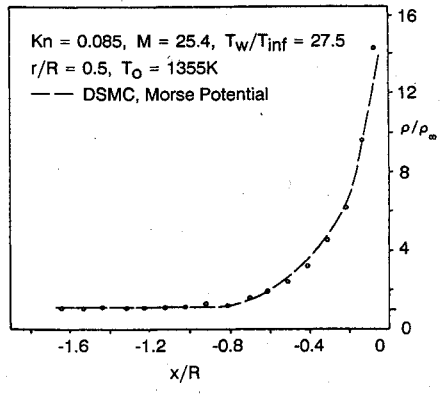


**Fig. 8 Measured and predicted density profiles off axis.**

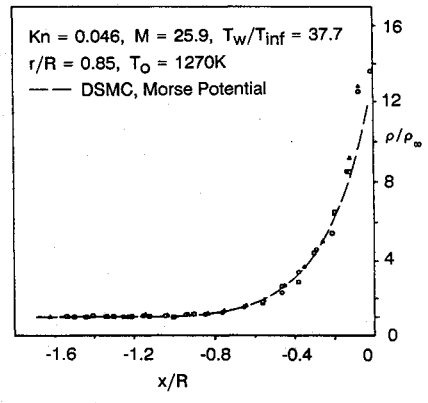


**Fig. 9 Measured and predicted density profiles off axis.**

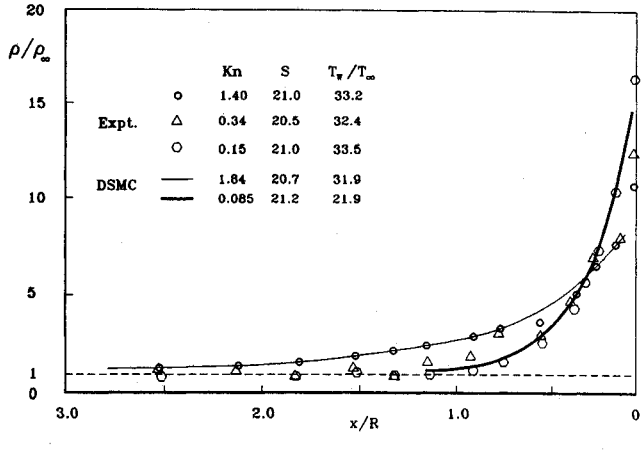


**Fig. 10 Measured and predicted density profiles along the axis for more rarefied flows.**

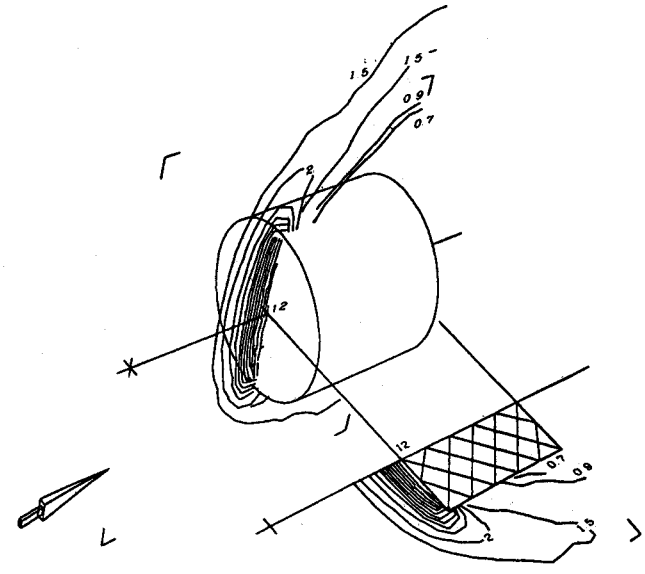

**Fig. 11 Computed density contours in the plane of symmetry and, in the foreground, perpendicular to that plane, for the body at 10-deg angle of attack; $M = 24.74$; $Kn = 0.064$.**

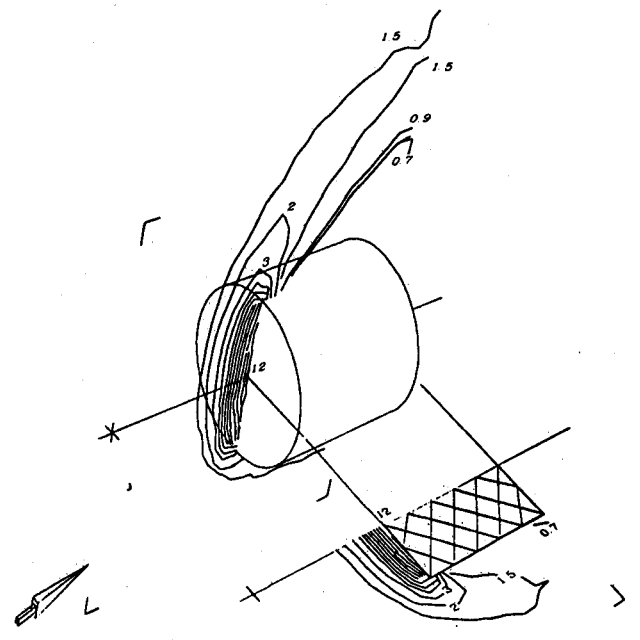

**Fig. 12 Computed density contours for 20-deg incidence; $M = 24.74$; $Kn = 0.064$.**

in Knudsen number, very little variation in the profile is seen. For clarity, individual test points have not been shown, but typical examples from which the curves have been derived can be seen in Figs. 7–9. Note that the scatter and run-to-run variations are small. Corresponding DSMC calculated density profiles are presented in these figures and close agreement is evident.

Further experiments were conducted with smaller models in order to obtain higher Knudsen numbers ranging up to 1.40. The measured and DSMC results are presented in Fig. 10. Once $Kn$ exceeds 0.15, the profiles, which hitherto only slowly changed with this parameter, begin to extend further into the undisturbed flow. The peak in density close to the body also

begins to fall. Although the freestream conditions for measured flows do not correspond exactly with those of the calculations, the trend with $Kn$ exhibited by the results corresponds very closely with the DSMC predictions, especially in the outer flow. Some experimental difficulties were experienced with the EBFT for the small models near the surface, and the data for $r/R < 0.2$ may be somewhat less precise.

A series of computed contour plots of density, rotational, and translational temperature are shown in Figs. 11–13 for angles of attack of 10, 20, and 40 deg for $Kn = 0.0645$. All variables are normalized with respect to their freestream values. Deliberately, no smoothing has been applied to these curves. The pictures show the contours for the plane of symmetry and, in the foreground, those for the perpendicular plane displaced laterally for clarity. Increasing the incidence causes the expected asymmetry in the flow patterns as the stagnation point moves from the axis to the lower windward side. As the incidence increases, the peaks in the density and translational temperature ahead of the body follow the location of the stagnation streamline and move from the axis of the body toward the windward edge of the front face. At the same time, the expansion on the leeward side extends further out into the flow.

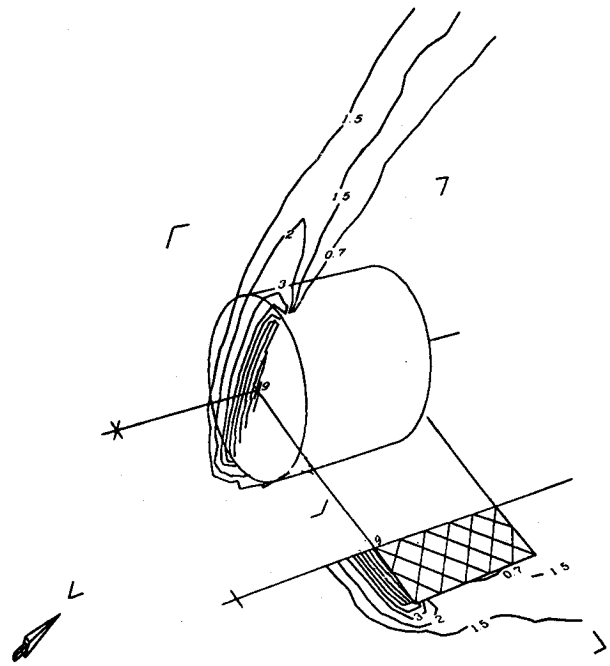


a) Density

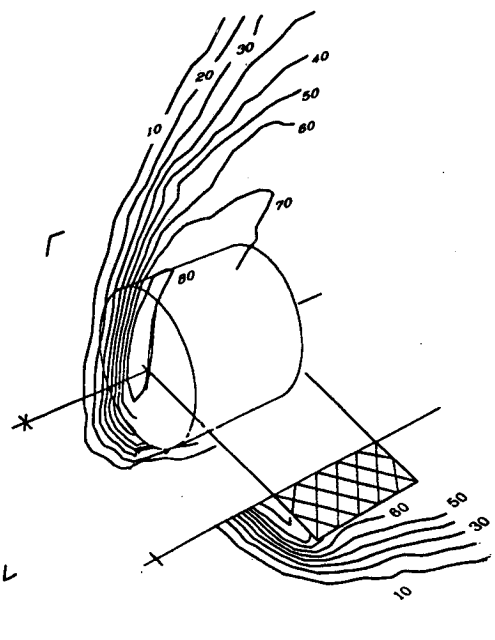


b) Rotational temperature

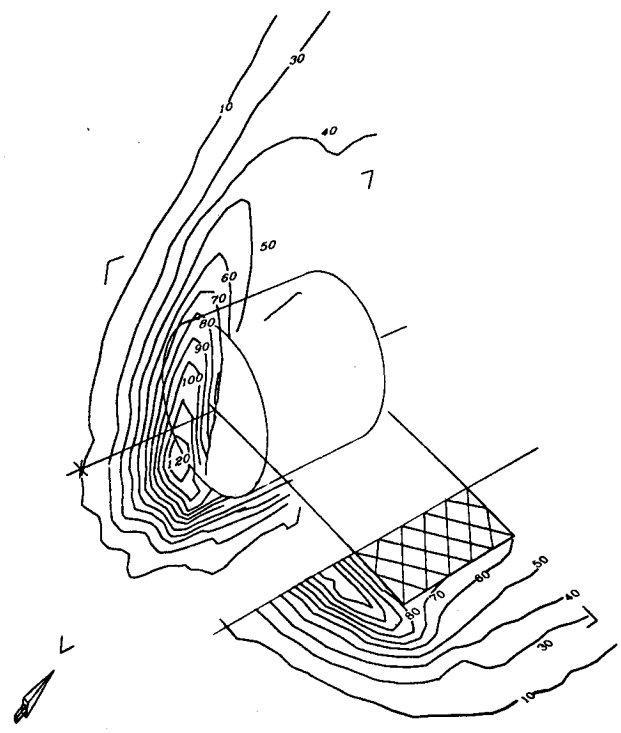


c) Translational temperature

**Fig. 13 Computed density and temperature contours for 40-deg incidence; $M = 24.74$; $Kn = 0.0645$.**

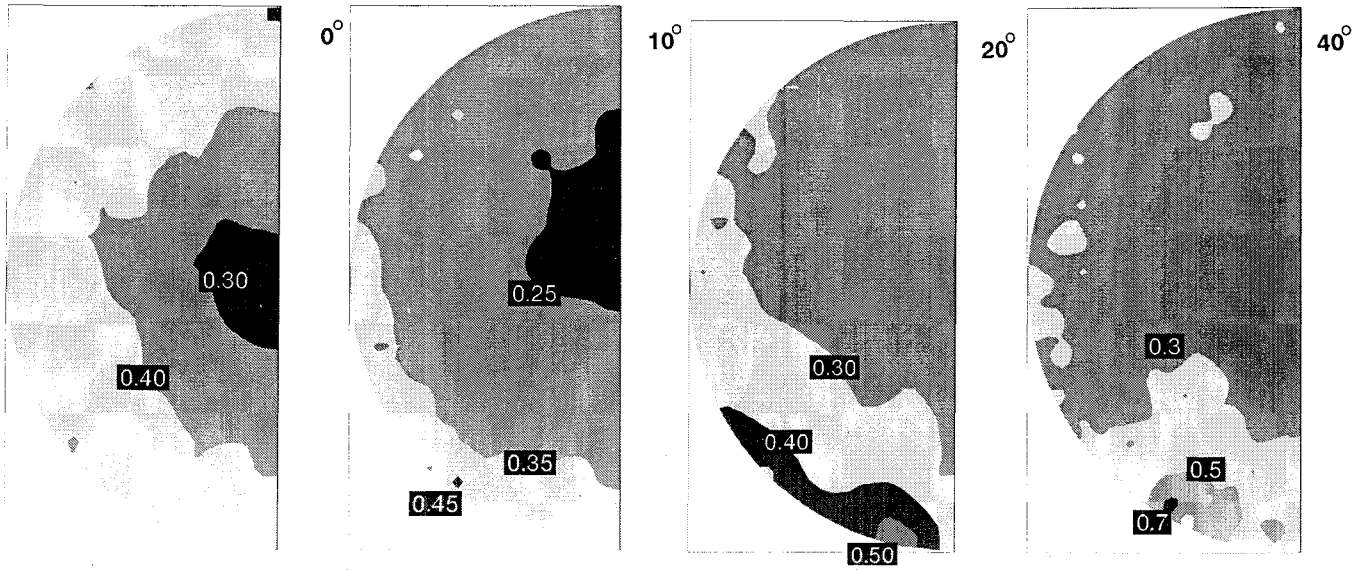


**Fig. 14 Computed distributions of Stanton number to the front face of the cylinder for 0-, 10-, 20- and 40-deg incidence at $M = 24.74$, $Kn = 0.0645$ (windward edge at the bottom).**

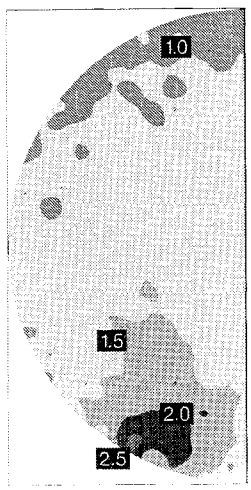


**Fig. 15 Corresponding pressure distribution on the front face for 40-deg incidence.**

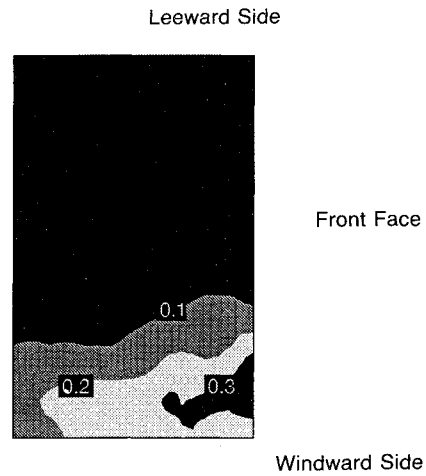


**Fig. 16 Calculated Stanton number distributions on the side of the cylinder at 40-deg incidence. The surface on one half of the cylinder has been "unwrapped" with the upwind end on the right of the picture.**

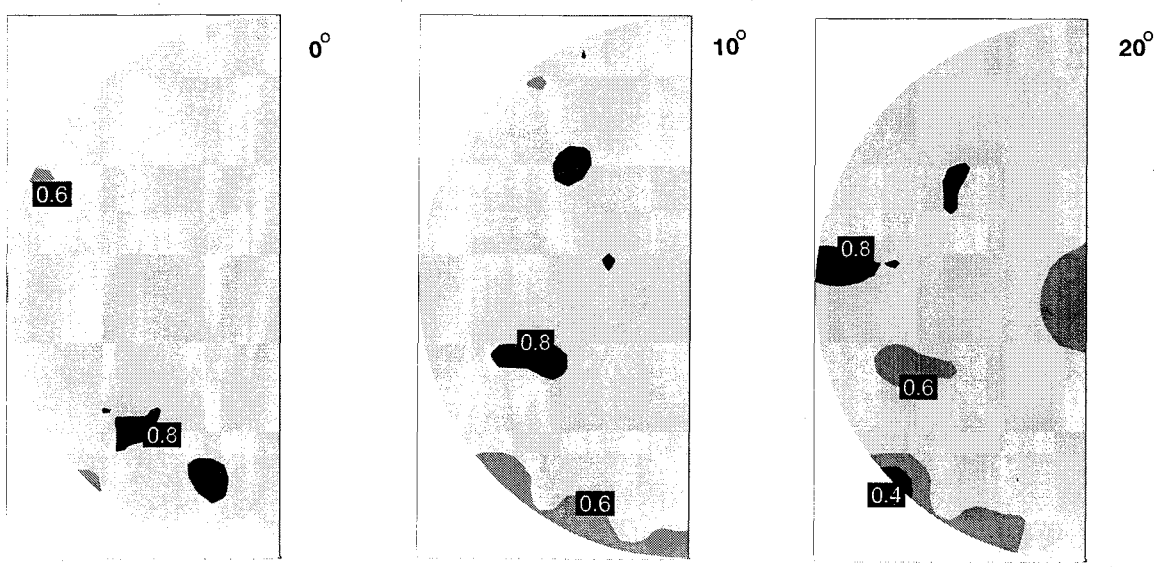


**Fig. 17 Distributions of Stanton number on the front face for a more rarefied flow; $Kn = 1.84$, $M = 24.74$ (windward edge at the bottom).**

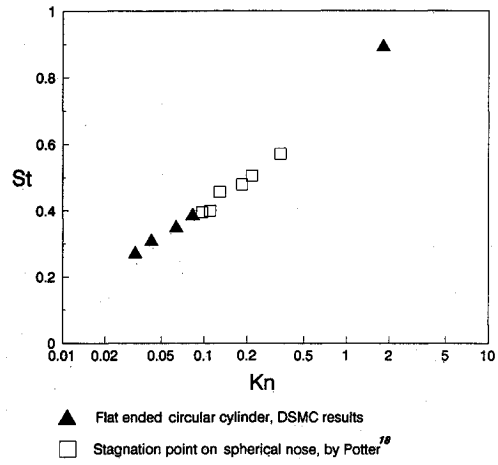


**Fig. 18 Variation with Knudsen number of the computed average Stanton number for heat transfer to the front face of the blunt cylinder. Also plotted are the values for the stagnation point of a spherical nose, reproduced from Potter.[18]**

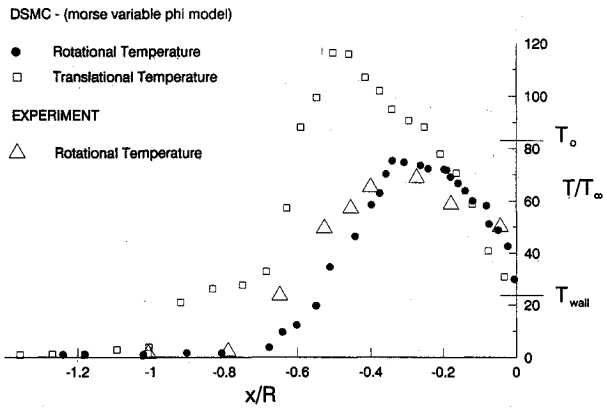


**Fig. 19 Comparisons between the measured and predicted rotational temperature variations ahead of the body at zero angle of attack along the axis; $M = 24.74$ and $Kn = 0.034$. The predicted translational temperature distribution is also shown.**

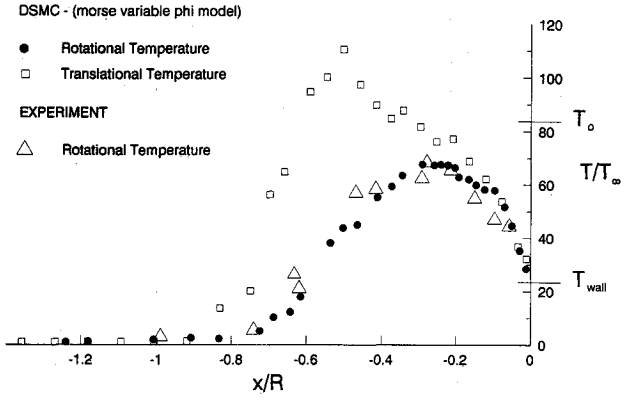


**Fig. 20 Similar comparisons to those of Fig. 19 but at $Kn = 0.043$.**

The lag in transferring translational energy to the internal modes leads to an interesting effect that is opposite to that observed for the translational temperature. The flow streaming toward the leeward edge of the front face has an extended path length, and energy thus continues to be transferred into the relatively cool internal mode, even though the translational temperature is falling. As a consequence, the peak in rotational temperature occurs toward the leeward side of the front face.

Distributions of the local Stanton number on the front face of the cylinder for several angles of attack at $Kn = 0.0645$ are shown in Fig. 14. Since the pattern is symmetrical, only half is shown. The windward edge is at the bottom of the plots and the leeward edge at the top. As the incidence increases, the heat flux rises on the windward side following the peak in translational temperature in the flow adjacent to it. However, an unexpected effect is seen at 20- and 40-deg angle of attack, where the maximum moves away from the stagnation point on the plane of symmetry. Instead two "hot spots" are formed on the edge on either side of the center plane. This behavior is echoed in the front face pressure distribution, an example of which, for 40-deg incidence, is given in Fig. 15. A carryover of this effect is seen in the Stanton number distributions on the cylindrical side of the body. Although the level of heat transfer is nearly an order of magnitude less than the average measured on the front face, peaks on either side of the center plane are observed that correspond in position to those on the front face (see Fig. 16).

An example of the heat transfer for a more rarefied flow ($Kn = 1.84$) is given in Fig. 17. Not surprisingly, the distribution tends toward a pattern more akin to the free molecular constant heat flux than would be expected for a plane surface. There is, in fact, a slight minimum where the hot spot was seen in the denser flow. Variations in the total heat transfer to the front face of the body have been calculated for the zero incidence case. In Fig. 18, the results are presented for the range of Knudsen numbers for which calculations were performed. Comparison is made with the Stanton numbers for the stagnation point on spherical noses in transitional flow given by Potter.[18] A close similarity between the trend of both sets of data is evident.

### Temperature

Comparisons between DSMC rotational temperature predictions and measurements made using the electron beam fluorescence technique for zero angle-of-attack flows are presented. The new calculated data are the result of long, carefully made computer runs. The comparisons are shown in Figs. 19 and 20 for $Kn$ 0.034 and 0.043, respectively. The correlation can be seen to be close, but there is a consistent trend towards the computation underpredicting on the upwind face of the compression ($x/R$ between $-0.6$ and $-0.4$) and overestimating the rotational temperature inboard of the peak ($x/r$ between $-0.2$ and 0). This would suggest that the coupling between the rotational mode and translational used in the calculations should be stronger.

## Concluding Remarks

From the comparisons made in this study of the flow about a bluff circular cylinder between DSMC calculation and experiments, the effectiveness of the numerical method to predict rarefied flow at a practical level is unquestionable. Density measurements show that over a range of Knudsen numbers the structure of the flow, which differs markedly from the continuum pattern, is accurately modeled. Only a few time-consuming rotational temperature measurements were possible. These indicate that the stochastic variable-$\phi$ restricted-enchange model, which is an extension of the Borgnakke-Larsen model that takes account of the variations in internal exchange with changing temperature, performed well. However, in the region where the rotational temperature is rising rapidly, it appears to underestimate the degree of coupling into the internal mode. The empirical constants used in the computational model for the internal energy exchange were derived from single cell relaxation simulations. The values used in the collision model were adjusted so that the simulated relaxation rates agreed closely with the experimental data for the range of expected temperatures.[11] The apparent inconsistency in the behavior of the internal energy exchange

model between the blunt cylinder and the relaxation simulations is thought to be attributable to the degree of nonequilibrium in the flow in the case of the former. The relaxation experiments were conducted in near equilibrium situations, whereas the flow approaching the front face of the cylinder is far from equilibrium and nonisotropic. It is not surprising that the gas appears to behave slightly differently in the two situations.

Three-dimensional computations have been successfully performed. Examination of the heat transfer patterns demonstrates that there is a noticeable and not unexpected change in the character of the flow over the range of Knudsen numbers considered, i.e., from 0.064 to 1.84. In the latter case, the fluxes show the characteristics of free molecular flow. In the more dense case, unexpected "hot spots" are seen away from the axis of symmetry and, hence, removed from the stagnation point.

The influence on the flow caused by unfreezing the vibrational exchange is difficult to resolve within the statistical scatter of the calculations. However, it would appear that consistently the heat transfer to the edges of the front face of the blunted cylinder was reduced when exchange to the vibrational mode was permitted.

## Acknowledgment

This work has been carried out with the support of the Procurement Executive of the British Ministry of Defence. The authors wish especially to acknowledge the assistance given by the Defence Research Agency (Aerospace Division), Farnborough, UK.

## References

[1]Bird, G. A., *Molecular Gas Dynamics*, Oxford University Press, Oxford, England, UK, 1976.

[2]Muntz, E. P., "Rarefied Gas Dynamics," *Annual Review of Fluid Mechanics*, No. 21, 1989, pp. 387–417.

[3]Harvey, J. K., "Direct Simulation Monte Carlo Method and Comparison with Experiment," *Thermophysical Aspects of Re-Entry Flows*, Vol. 103, Progress in Astronautics and Aeronautics, AIAA, New York, 1986, pp. 25–43.

[4]Davis, J., Dominy, R. G., Harvey, J. K., and Macrossan, M. N., "Evaluation of Some Collision Models Used in the Monte-Carlo Calculation of Diatomic Rarefied Flows," *Journal of Fluid Mechanics*, Vol. 135, 1983, pp. 355–371.

[5]Macrossan, M. N., "Diatomic Collision Models Used in the Monte-Carlo Direct Simulation Method Applied to Rarefied Hypersonic Flows," Ph.D. Thesis, Univ. of London, London, 1983.

[6]Bird, G. A., "Monte Carlo Simulation in an Engineering Contex," *Rarefied Gas Dynamics*, edited by S. S. Fisher, Vol. 74, Progress in Astronautics and Aeronautics, AIAA, New York, 1981, pp. 239–256.

[7]Borgnakke, C., and Larsen, P. S., "Statistical Collision Models for Monte-Carlo Simulation of Polyatomic Gas," Dept. of Fluid Mechanics, Technical Univ. of Denmark, Rept. AFM 73-08, 1973.

[8]Larsen, P. I., and Borgnakke, C., "Statistical Collision Model for Simulating Polyatomic Gas with Restricted Energy Exchange," *Rarefied Gas Dynamics,* edited by Backer and Fiebig, Paper A7, DFVLR Press, Portz-Wahn, Germany, 1974.

[9]Davis, J., "An Experimental Study to Evaluate and Develop the Direct Simulation Method as Applied to Rarefied Hypersonic Flow Fields," Ph.D. Thesis, Univ. of London, London, 1978.

[10]Pullin, D. I., "Kinetic Models for Polyatomic Molecules with Phenomenological Energy Exchange," *Physics of Fluids*, Vol. 21, No. 2, 1979, pp. 209–216.

[11]Carnevale, E. H., Cary, C., and Larsen, G., "Ultra-Sonic Determination of Rotational Collision Numbers and Vibrational Relaxation Times of Polyatomic Gases at High Temperatures," *Journal of Chemical Physics*, Vol. 47, No. 8, 1967, p. 2829.

[12]Lambert, J. D., *Vibrational and Rotational Relaxation in Gases*, Clarendon Press, Oxford, England, UK, 1977.

[13]*Handbook of Chemistry and Physics*, editor-in-chief R. C. Weast, 66th edition, CRC Press, Boca Raton, FL, 1985-1986.

[14]Huber, K. P., and Hertzberg, G., *Molecular Structure*, Vol. 4, "Constants of Diatomic Molecules," Van Nostrand Reinhold, New York, 1978.

[15]Dominy, R. G., "Rarefied Hypersonic Shock Wave and Blunt Body Flows," Ph.D. Thesis, Univ. of London, London, 1987.

[16]Smith, R. B., "$N_2$ First Negative Band Broadening Due to Electron Beam Excitation," *Rarefied Gas Dynamics*, edited by Trilling and Wachman, Vol. 2, Academic Press, New York, 1969, pp. 1713–1749.

[17]Cattolica, R. J., Schmitt, R. L., and Palmer, R. E., "Feasibility of Flight Experiments and Instrumentation Hardware for In-Flight Hypersonic Boundary-Layer Measurement," Sandia National Lab., Livermore, CA, Rept. SAND89-UC-13, 1989.

[18]Potter, J. L., "Transitional Hypersonic Aerodynamic Simulation and Scaling," *Thermophysical Aspects of Re-Entry Flows*, Vol. 103, Progress in Astronautics and Aeronautics, AIAA, New York, 1986.